JMEPEG (2008) 17:572–579
DOI: 10.1007/s11665-007-9173-5

1059-9495/$19.00

High-Temperature Deformation and Ductility of a Modified 5083 Al Alloy

Ehab A. El-Danaf, Abdulhakim A. Almajid, and Mahmoud S. Soliman

(Submitted November 14, 2006; in revised form June 3, 2007)

The high-temperature deformation of a 5.5% Mg and 0.6% Ca modified 5083 aluminum alloy was investigated in the temperature range from 573 to 723 K at strain rates in the range of 10^{-5}-10^{-1} s^{-1}. Ca was added to form an insoluble second phase in the range of temperatures tested to improve the high-temperature characteristics of this alloy. It was shown that the deformation behavior of the alloy could be divided into two regions with stress exponent, *n* of 3.5 and 13 at low and high strain rates, respectively. The apparent activation energy determined in both regions suggested that the deformation process is diffusion controlled in both regions. The slightly high value of *n* at the low-strain rate region (viscous glide) was attributed to the presence of threshold stress. The values of threshold stress showed an exponential increase with decreasing temperature and a dependence with an energy term *Q*o = 16.5 kJ mol^{-1}. Analysis of creep data in terms of threshold stress and using diffusivity of Mg in normalizing the strain rates, revealed two types of deformation behavior. At high values of normalized strain rate ($\dot{\varepsilon}kT/DGb > 10^{-9}$), a high value of stress exponent of *n* = 10 is observed, and the exponential law creep takes place. At low normalized strain rates $\leq 10^{-9}$, the *n* value is 3 and the true activation energy, *Q*, is equal to 123 kJ mol^{-1} suggesting viscous glide of dislocations as rate-controlling mechanism. Enhanced ductility has been observed in the region of viscous-glide controlled deformation as a result of high strain-rate sensitivity.

Keywords activation energy, Al-alloy 5083, ductility, hot deformation, threshold stress, viscous glide

1. Introduction

High-temperature deformation of pure metals and substitutional metallic solid solutions is usually described by a power function; in the so-called power law regime, as:

$$\dot{\varepsilon} = A\sigma^n \exp\left(\frac{-Q_a}{RT}\right), \quad \text{(Eq 1)}$$

where $\dot{\varepsilon}$ is the strain rate, σ is the stress, n is the stress exponent, Q_a is the apparent activation energy, R is the universal gas constant, T is the absolute temperature and A is a constant. The value of n and other characteristics were used to classify metals and alloys (Ref 1-4). For Al-Mg alloys (Ref 5-10) and Al-Cu alloys (Ref 11-13), which exhibit large solid solution hardening (high atomic-misfit parameter), the measured values of n are close to 3, and are characterized by solute drag mechanism resulting from elastic interaction between dislocations and solute atoms due to the size effect. This type of behavior has been termed as class I or alloy class (Ref 1, 3). On the other hand, for pure metals and some solid solution alloys, usually with low atomic-misfit parameter, the values of n are close to 5 and the strain rate is a function of stacking fault energy. This behavior is termed as class II or pure metal class (Ref 1, 3). It is believed that some form of dislocation climb is the rate-controlling process.

Later, it was noticed that solute drag or viscous glide (n = 3) is rate-controlling at intermediate stress region in alloy-class alloys. However, when the stress is decreased or increased above a critical value, transition to a low stress region or high stress region, the value of n starts to deviate from 3 reaching a value of 5 at both regions (Ref 8-14). The change in the value of n is usually attributed to the change in the rate-controlling process. At extremely high stresses the creep-power law breaks down.

It was suggested that dislocation climb and viscous glide are two sequential processes in solid-solution alloys and that the slower process controls the deformation mechanism under the imposed experimental conditions (Ref 3, 15-17). It was also suggested that other viscous drag processes can operate sequentially with the solute-drag mechanism, but the contribution of these processes to the total drag force depend on the alloy system (Ref 14, 18).

The hot formability of aluminum alloys has been extensively studied in the last decades. The majority of these studies have investigated alloys produced by ingot metallurgy (IM) (Ref 19-27); others have also examined the high-temperature deformation of alloys produced by powder metallurgy (PM) and of aluminum-based metal-matrix composites (Ref 28-41). These materials are characterized by the presence of the threshold stress σ_o, resulting from the interaction of the fine-dispersed particles in these alloys with the moving lattice dislocations. Under this condition, the deformation process is not driven by the applied stress, but rather by an effective stress σ_e ($=\sigma - \sigma_o$). However, a recent study (Ref 42) on the creep behavior of a commercial purity 5083 Al alloy over a wide range of stresses and temperatures did not report the presence

Ehab A. El-Danaf, Abdulhakim A. Almajid, and **Mahmoud S. Soliman**, Department of Mechanical Engineering, College of Engineering, King Saud University, P.O. Box 800, Riyadh 11421, Saudi Arabia. Contact e-mail: solimanm@ksu.edu.sa.

of threshold stress and gave a high constant value for n (=5.4) and a high value for the activation energy (=210 kJ mol^{-1}) as compared to the activation energy for diffusion of Mg (115-130 kJ mol^{-1}) in Al (Ref 43, 44) and self diffusion in Al (143 kJ mol^{-1}) (Ref 45).

The objective of the present study is to examine, in detail, the high-temperature deformation of a Ca-modified 5083 Al alloy over a wide range of stresses, strain rates, and temperatures to examine the presence of the threshold stress and find out the rate-controlling mechanisms in the deformation of IM alloys. The Ca addition was made in order to have an insoluble second-phase (Al_4Ca) in the range of temperatures tested to improve the high-temperature characteristics of this alloy (Ref 46). In addition, the ductility of the present alloy will be investigated.

2. Experimental Procedure

High-temperature tensile tests were carried out on a modified 5083 aluminum alloy, whose composition in wt% is as follows: 5.5 Mg, 0.85 Mn, 0.6 Ca, 0.4 Si, 0.19 Fe, 0.12 Cr and the rest is Al. The alloy was supplied as cold-rolled plate. Flat tensile specimens of 12 mm gage length and 5×3 mm cross-section were machined such that the tensile axis was parallel to the rolling direction. The specimens were annealed at 723 K for 1 h to remove the effects of machining and to produce a stable uniform grain size of about 20 μm. The main mechanical properties at room temperature were the yield strength of 220 MPa, the tensile strength of 337 MPa and the elongation of 27% for the annealed condition. The tension tests were carried out using an Instron machine, with a resistance furnace containing three heating zones. All specimens were tested in air and soaked in the furnace at the testing temperature for 15 min prior to testing to establish thermal equilibrium. Four different temperatures were used namely, 573, 623, 673, and 723 K. In addition, at 723 K, strain rate jump tests were conducted to check for data reproducibility and have more data points using single sample. The temperature was controlled using a thermocouple connected to the middle of the gauge section and was kept to within ±2 K. At each temperature six different constant cross-head speeds were used ranging from 0.02 to 50 mm/min, which corresponds to an initial strain rates in the range of 2.7×10^{-5} s^{-1} to 6.9×10^{-2} s^{-1}. The strain rates quoted thereafter represent the initial strain rates calculated from the initial gage length of the specimens. The load displacement data were obtained and the corresponding true stress-strain curves were calculated.

3. Results

3.1 True Stress-Strain Curves

Figure 1 shows the true stress-strain response at 573, 623, and 673 K for different initial strain rates. In order to avoid repetition, some of the stress-strain curves, obtained at 723 K

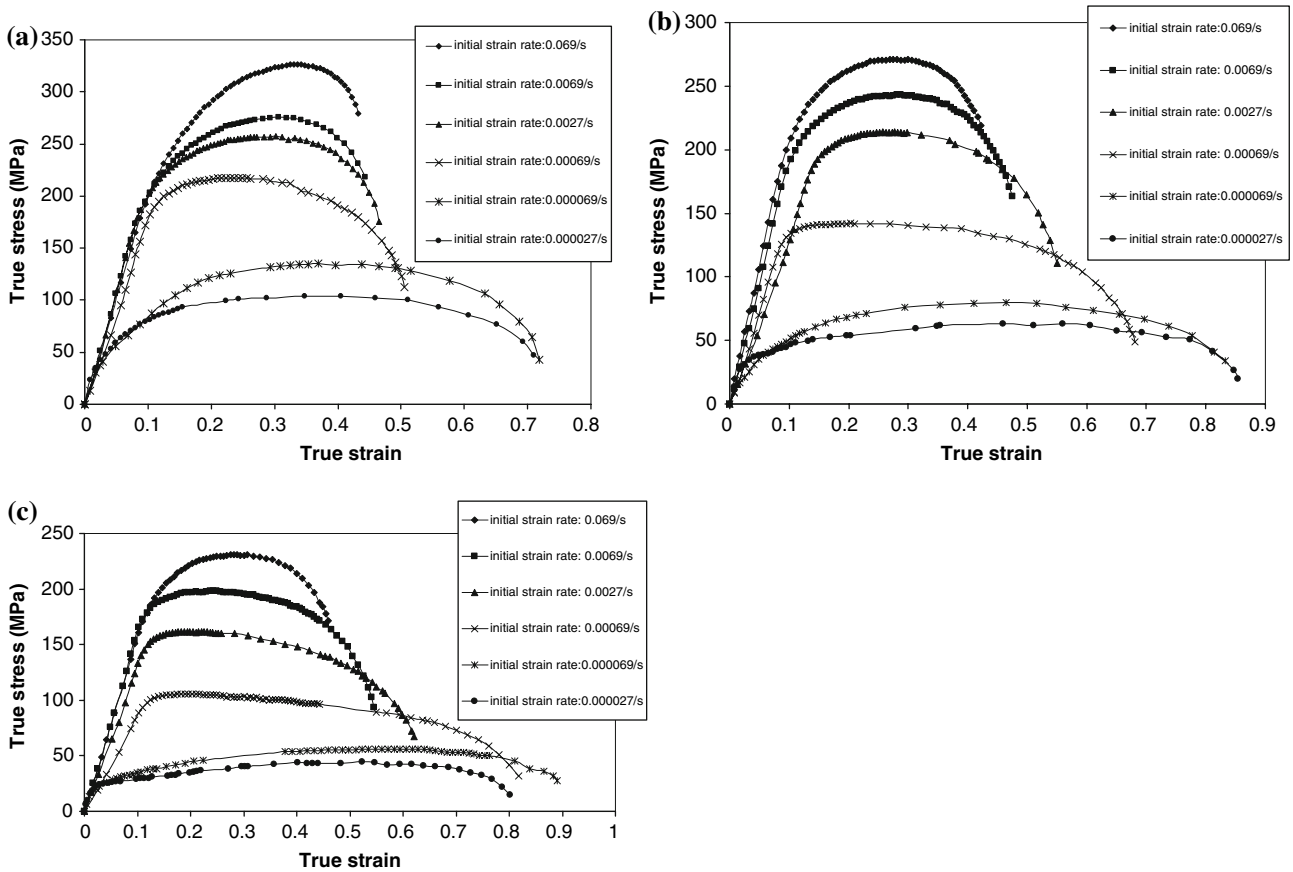

Fig. 1 (a-c) True stress-true strain response at 573, 623, and 673 K respectively, at different strain rates

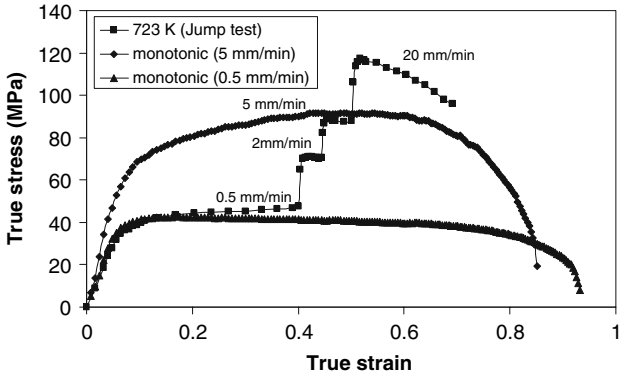

Fig. 2 True stress-true strain response obtained for a strain rate jump test at a temperature of 723 K as well as two monotonic tests conducted at the same temperature and at two of the velocities

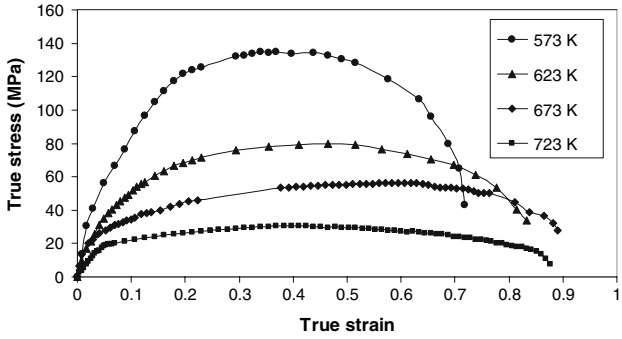

Fig. 3 True stress-true strain response at different temperatures at a constant strain rate of 6.9×10^{-5} s^{-1}

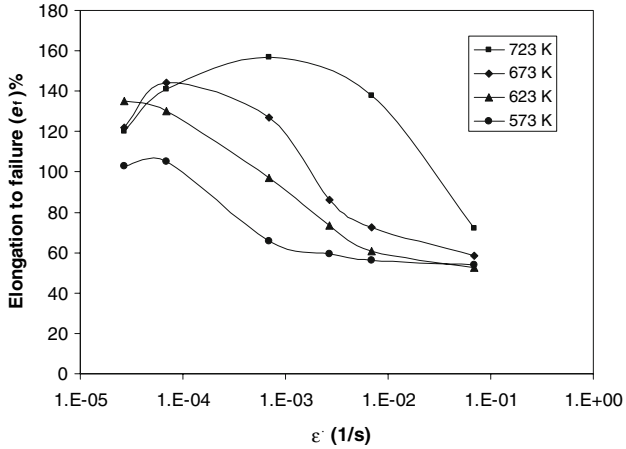

Fig. 4 Elongation at failure, e_f% as a function of temperature and strain rate

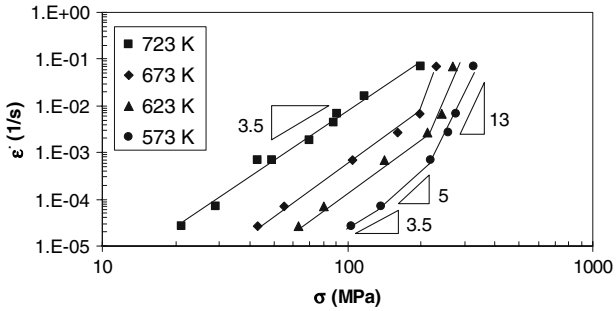

Fig. 5 Stress dependence of the strain rate at different temperatures, showing the value of stress exponent at different regions

are presented in Fig. 2 and 3. The results show the high strain rate sensitivity exhibited by the alloy at these temperatures. The true stress-strain response can be divided into three regions. Region I is the strain-hardening region, where the stress increases with strain until it reaches almost constant value. Region II represents the steady-state stress at the applied strain rate. The steady state is reached after strain ≥0.2. In region III, necking and/or cracking occurs leading to a decrease in the flow stress and thereafter fracture. These experiments, which are conducted at constant initial strain rate were used to determine ductility (elongation percent at fracture). Figure 2 shows the strain-rate jump test conducted at 723 K, in which the same sample was subjected to different strain rates by increasing the testing speed at specified intervals, and also shown are two monotonic tests at the same temperature conducted at two different velocities similar to the ones used in the jump test. Figure 3 shows the effect of temperature on true stress-strain curves at constant strain rate of 6.9×10^{-5} s^{-1}. It is seen that the steady state (region II) is reached after same amount of strain irrespective of temperature ($\varepsilon\sim0.2$), and that elongation percent at fracture increased with temperature until 673 K and decreased slightly at 723 K.

3.2 Ductility

Figure 4 shows the results of ductility measurements in which the elongation at fracture e_f% (=$\Delta L_f/L_o$, where ΔL_f is the increase in length at fracture and L_o is the initial length of the specimen), is plotted as a function of initial strain rate $\dot{\varepsilon}$ at various testing temperatures. An examination of the figure suggests that the maximum ductility increases with increasing temperature and the ductility decreases with increasing strain rate. In addition, the e_f% values show a maximum at 723 K (∼160%) and the values decreases slowly with strain rate as compared to the sharp decrease at 573 K. At the highest strain rate of 6.9×10^{-2} s^{-1}, the value of e_f% for 573, 623, and 673 K is independent of temperature and reaches a low value of about 60%, at this strain rate and at 723 K the e_f% exhibited a higher value of about 80%.

3.3 Stress Dependence of Strain Rate

The stress dependence of the strain rate under steady-state condition at constant temperature is determined by plotting the strain rate, $\dot{\varepsilon}$as a function of the steady state stress, σ on a double logarithmic scale. Figure 5 shows this form of plot for four different temperatures 573, 623, 673, and 723 K. Examination of the data of this figure reveals the following. The data points at 723 K falls on a segment of straight line with slope of 3.5. Second, at 673 and 623, the data points fall on two segments of straight lines with slope ≈3.5 at low strain rates (low stresses) and slope of ≈13 at high strain rates (high stresses). Third, data points at 573 K fall on three segments of straight lines with slope of ≈3.5, ≈5, and ≈13 with increasing strain rate. It can be noticed that the data points are limited in the first two regions. It is also noticed that the region with stress exponent $n\approx3.5$ is extended to high strain rates with increasing

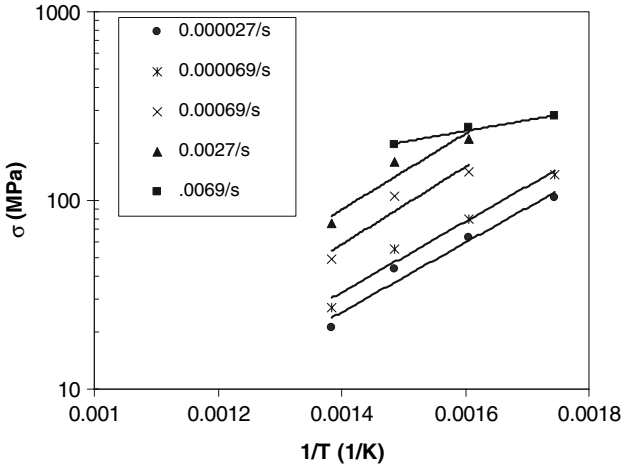

Fig. 6 A semilogarithmic plot of stress vs. the reciprocal of absolute temperature at various strain rates

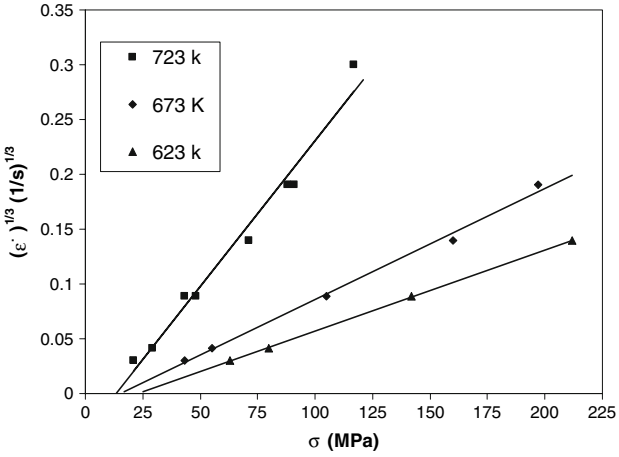

Fig. 7 Double linear plot for $\dot{\varepsilon}^{(1/3)}$ vs. stress at different temperatures

temperature; it is extended to $\dot{\varepsilon}$ of 7×10^{-3} s^{-1} at 673 K as compared to 7×10^{-5} s^{-1} at 573 K.

3.4 Apparent Activation Energy

Using Eq 1, the apparent activation energy Q_a can be calculated at constant strain rate as

$$Q_a = nR\left[\frac{\partial \ln \sigma}{\partial\left(1/T\right)}\right]_{\dot{\varepsilon}} \quad \text{(Eq 2)}$$

Figure 6 shows a plot of log σ vs. $(1/T)$. The data points at constant strain rate fall on a segment of straight line, whose slope is equal to $\left(\frac{Q_a}{2.3nR}\right)$, which gives Q_a a value of 130 and 143 kJ mol^{-1}, for low and high strain rate regions, respectively. In calculating Q_a, the values of n were taken as 3.5 and 13 for low strain rate region and high strain-rate region, respectively.

4. Discussions

4.1 Threshold Stress

It is shown in Fig. 5 that the low stress region has a value of $n \approx 3.5$. This value is higher than what is usually reported for binary Al-Mg alloys (n = 3). The reason for this discrepancy may arise from the presence of threshold stress which is not clearly observed because of the limited range of strain rate covered in the present experiments. This possibility is explored by plotting $\dot{\varepsilon}^{1/3}$ vs. σ using double linear scale as shown in Fig. 7. The data points for each temperature fall on a segment of straight line and the extrapolation of these lines to zero strain rate gives the value of σ_o at each temperature. The values of σ_o are 13, 16, and 24 MPa at 723, 673, and 623 K, respectively. Two data points are available only at 573 K so the value of the threshold stress cannot be determined from the experimental results at this temperature. The temperature dependence of normalized threshold stress is plotted in Fig. 8 as (σ_o/G) vs. $1/T$ on semilogarithmic scale. The value of the shear modulus, G (N/m^2) for the alloy as a function of temperature is taken as (Ref 47)

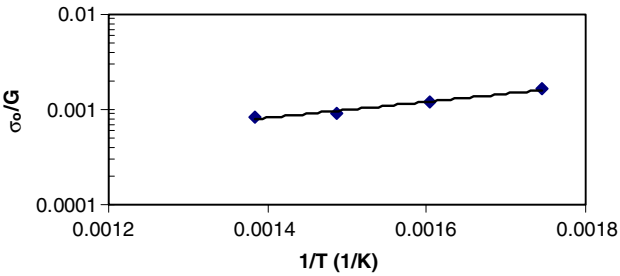

Fig. 8 Semilogarithmic plot for normalized threshold stress vs. the reciprocal of absolute temperature

$$G = 4.7859\times10^{10} - 1.3571\times10^{8}T + 2.6402\times10^{5}T^2 - 190.84T^3 \quad \text{(Eq 3)}$$

The data points of (σ_o/G) fall on a straight line that the relationship can be expressed as (Ref 28-30):

$$\frac{\sigma_o}{G} = B_o \exp\left(\frac{Q_o}{RT}\right) \quad \text{(Eq 4)}$$

where B_o is a constant. The value of Q_o as inferred from Fig. 8 is 16.5 kJ mol^{-1} which is in good agreement with the value reported for a modified 5083 alloy (18 kJ/mol) (Ref 27) though the present values for σ_o are slightly higher than those reported earlier. Due to the limited data in the low-stress region at 573 K, the value of σ_o at this temperature was estimated, using Eq 4, as 34.6 MPa. The present results along with previous studies (Ref 27, 37) suggest that σ_o is a function of temperature only and it decreases with increasing temperature. It was shown recently (Ref 37, 41) even under the presence of two regions of deformation, viscous glide (n = 3) and high stress region with n close to 5, the value of the threshold stress is the same in both regions. Therefore, the value of σ_o was taken as a constant value at each temperature though the datum points at high stress region were not included in the calculation of σ_o. When the strain rates are plotted as a function of the effective stress, the stress exponent n inferred at low strain rates is 3, while it has a value of 12 at high stresses, as shown in Fig. 9.

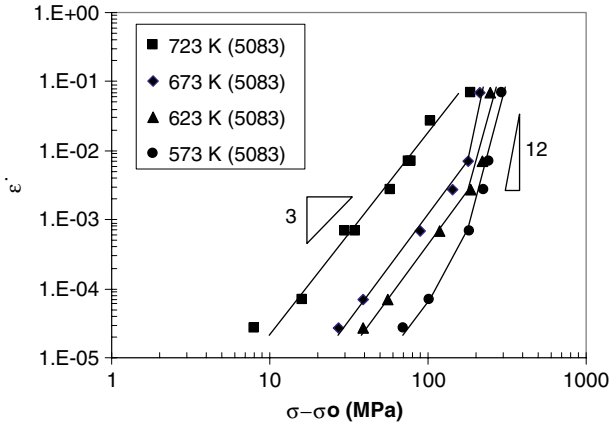

Fig. 9 A double logarithmic plot for effective stress dependence on strain rate

4.2 True Activation Energy

Under the presence of threshold stress, Eq 1 can be modified such that the applied stress is replaced by an effective stress. This equation when written in the normalized form is given by:

$$\frac{\dot{\varepsilon}kT}{DGb} = A_o\left(\frac{\sigma - \sigma_o}{G}\right)^n, \qquad \text{(Eq 5a)}$$

with

$$D = D_o \exp\left(\frac{-Q}{RT}\right), \qquad \text{(Eq 5b)}$$

where k is Boltzmann's constant, b is the magnitude of Burgers vector, A_o is a dimensionless constant, Q is the true activation energy for the diffusion process that controls the deformation mechanism and D_o is a frequency factor. Equation 5, at constant strain rate, can be rearranged in the form

$$\exp\left(\frac{Q}{RT}\right) = C\left(\frac{G}{T}\right)\left(\frac{\sigma - \sigma_o}{G}\right)^n, \qquad \text{(Eq 6)}$$

where C is a constant. Taking the natural logarithm of Eq 6 and differentiating with respect to $\left(\frac{1}{T}\right)$, the value of Q can be written as:

$$Q = R\frac{\partial \ln\left[\frac{G}{T}\left(\frac{\sigma-\sigma_o}{G}\right)^n\right]}{\partial\left(\frac{1}{T}\right)} \qquad \text{(Eq 7)}$$

Equation 7 is used to calculate the true activation energy in the low stress region by plotting $\log\left[\frac{G}{T}\left(\frac{\sigma-\sigma_o}{G}\right)^3\right]$ vs. $\left(\frac{1}{T}\right)$ as shown in Fig. 10. The value of Q was determined at four various strain rates in the temperature range of 573-723 K. As shown in the figure data points fall on segments of parallel straight lines giving Q a constant value independent of strain rate. The average value of Q was calculated as 123 kJ mol^{-1}. This value is very close to that reported for diffusion of Mg in Al (115-130 kJ mol^{-1}) (Ref 43, 44). The true activation energy at high stress region cannot be unambiguously identified because of limited data points at temperatures above 573 K.

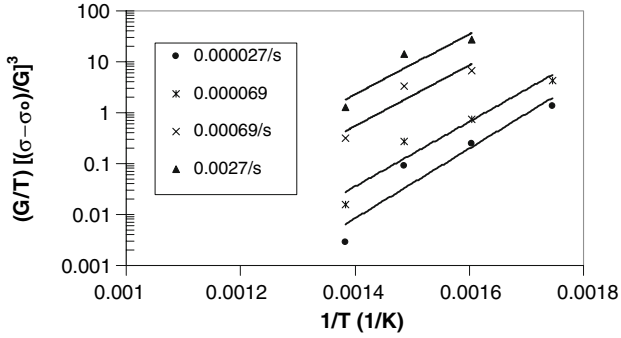

Fig. 10 Semilogarithmic plot of $(G/T)[(\sigma - \sigma_o)/G]^3$ vs. $(1/T)$ for calculating the true activation energy

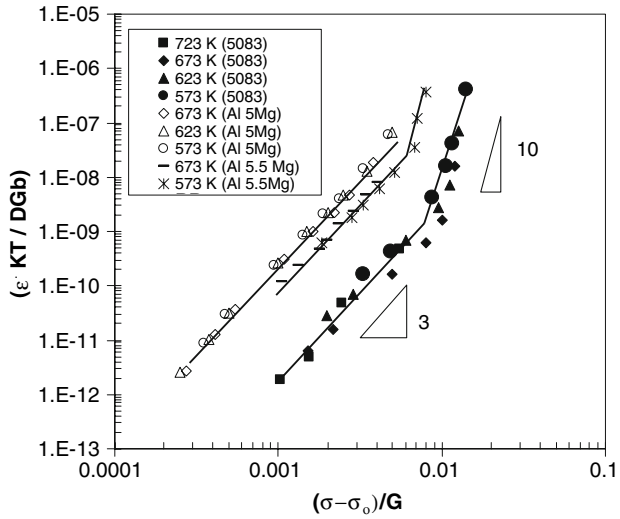

Fig. 11 Normalized strain rate vs. normalized effective stress for modified 5083 Alloy tested in the present study and Al-5.5 Mg-0.5Mn alloy (Ref 48) and normalized strain rate vs. normalized stress (σ/G) for Al-5Mg binary alloy (Ref 49) tested at same temperatures

4.3 Normalized Strain Rates

Because of the similarity between the value of Q at low strain rates and that for the diffusivity of Mg in Al, the diffusion coefficient for diffusion of Mg in Al; $D_{Mg} = 0.0632 \times 10^{-4}\exp\left(\frac{-115\times10^3}{RT}\right)$ m^2 s^{-1} (Ref 43), was used in normalizing the data of the alloy as presented in Fig. 9. Figure 11 gives the normalized creep rate $(\dot{\varepsilon}kT/DGB)$ vs. the normalized effective stress $\left(\frac{\sigma-\sigma_o}{G}\right)$. As shown in the figure, the data points coalesce on two segments of straight lines with slope 3 at low stresses and slope 10 at high stresses. The clustering of data points at high stress region on a single segment of straight line suggest that the true activation energy in this region, is not far from that of diffusion of Mg in Al (115 kJ mol^{-1}). Also included in Fig. 11, for the purpose of comparison, the data of two Al alloys with nearly same Mg content, namely, Al-5.5 Mg-0.5 Mn alloy (Ref 48) and Al-5 Mg binary alloy (Ref 49) tested at same temperatures. In normalizing the data for Al-5 Mg, the shear modulus and self diffusivity of Al were used (Ref 27) whereas the diffusivity of Mg in Al and the shear modulus (Eq 3) were used in normalizing the data of the second alloy, in the same way the

data of 5083 alloy was normalized. It is worth mentioning that Al-5.5 Mg-0.5 Mn alloy has 0.47% Mn compared to 0.85% of the present alloy and almost zero content of the other alloying elements. It can be seen that the addition of transition elements such as Mn, Cr, Fe and the presence of Ca has clearly increased the strength of the modified 5083 alloy.

4.4 Power Law Breakdown

The transition from viscous glide region (n = 3) to a region of high stress exponent (n = 10) is due to transition in the rate-controlling process. The high value of n at high stresses cannot be attributed to pipe diffusion or dislocation climb but rather to the exponential dependence of strain rate on the applied stress. The high stress region is usually attributed to the breakaway of dislocations from their solute atom atmospheres. For alloys showing threshold stress the value of stress required for atoms to breakaway from their solute atom atmospheres is given by (Ref 17, 32)

$$\left(\frac{\sigma - \sigma_o}{G}\right) = \frac{0.1ce^2Gb^3}{kT} \qquad \text{(Eq 8)}$$

where c is the Mg concentration in atomic percent (=0.06), e is the atomic misfit parameter (=0.12). Equation 8 gives the effective normalized breakaway stress a value of 5×10^{-3} at 623 K. This value is slightly lower than that inferred from Fig. 11.

At 573 K, the value of n changes from 3 to 5 and to 12. In pure metals and alloys of the metal class, it was suggested (Ref 1) that the breakdown of creep power law occurs at $\left(\frac{\dot{\varepsilon}}{D}\right) = 10^{13}\ \mathrm{m}^{-2}$. The transition in n above 5 was noticed at 573 K at strain rate of $2\times10^{-3}\ \mathrm{s}^{-1}$ which gives $(\dot{\varepsilon}/D)$ a value of $9\times10^{12}\ \mathrm{m}^{-2}$ where D is the diffusivity of Mg in pure Al. This value is in good agreement with the prediction.

4.5 Origin of Threshold Stress

The origin of the threshold stress is attributed to the presence of Al_3Cr, Al_6Mn, and Al_4Ca incoherent particles. TEM observations clearly confirmed the existence of a strong attractive interaction between particles and mobile lattice dislocations (Ref 27). A recent study of in situ TEM high-temperature deformation (Ref 50) was used to investigate the mechanisms by which dislocations and dislocation arrays in low-angle subgrain boundaries interact with semicoherent particles in Al alloys. The bypass mechanism involves interaction of the lattice dislocation with the particle-matrix interfacial dislocations, and the rate-limiting step is the detachment of the lattice dislocation from the particle. This limiting step may involve the reconstruction of the lattice dislocation from the interfacial dislocations at the detachment point. The interaction alters the interfacial structure which will influence subsequent dislocation-particle interactions.

4.6 Correlation with Hyperbolic Sine Equation

It was suggested that a hyperbolic sine equation could be used to describe the stress dependence of strain rate over wide range of stress that covers power law and power law breakdown (PLB) regions. This equation is written in the form (Ref 4, 19, 51):

$$\dot{\varepsilon} = A' \exp\left(\frac{-Q}{RT}\right)(\sinh \alpha\sigma)^n \qquad \text{(Eq 9)}$$

where A' and α are constants, Q is the apparent activation energy and n is the stress exponent at power law region. The values of α and n can only be determined when the data at both power law and PLB regions are available. Using the high stress data at 573 K that has enough data points that clearly manifests the PLB region, and taking $n = 3$, as observed at low stresses, the value of α is determined as $0.011\ \mathrm{MPa}^{-1}$, which is within the range observed for Al alloys (Ref 51). Figure 12 shows the relation between $\dot{\varepsilon}$ and sinh $\alpha\sigma$ at various temperatures. The data points at each temperature fall on a segment of straight line with slope of 2.8 which is less than that observed at low stress region. The present study suggests the presence of threshold stress σ_o and the data of the alloy is plotted as $\dot{\varepsilon}$ vs. sinh $\alpha(\sigma-\sigma_o)$ in Fig. 13. The data points fall on a group of parallel segment lines with a slope of 2.6. To compare the present data with those published for Al alloys, and taking the effect of σ_o into account Eq 9 is written in a normalized form

$$(\dot{\varepsilon}kT/DGb) = A_o \sinh\left[\alpha'(\sigma - \sigma_o)/G\right]^n \qquad \text{(Eq 10)}$$

The normalized strain rate $(\dot{\varepsilon}kT/DGb)$ is plotted vs. sinh $[\alpha'(\sigma-\sigma_o)/G]$ on double logarithmic scale in Fig. 14. The threshold stress for Al-5.5 Mg-0.5 Mn alloy (Ref 48) was calculated at present as 8.3 and 13.4 MPa at 673 and 573 K, respectively. The values of α' for this alloy and the present 5083 alloy are calculated to be 321 and 236, respectively. It is clear that the value of α' is not constant and alloy dependent and it

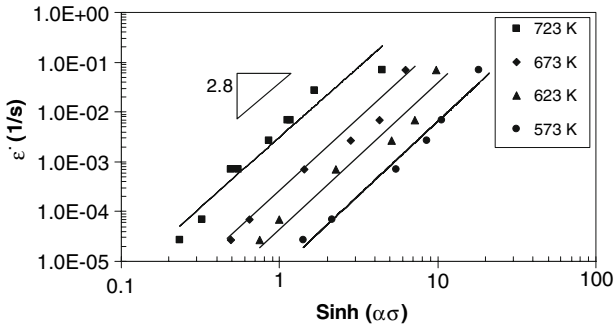

Fig. 12 Relation between $\dot{\varepsilon}$ and sinh $\alpha\sigma$ at various temperatures

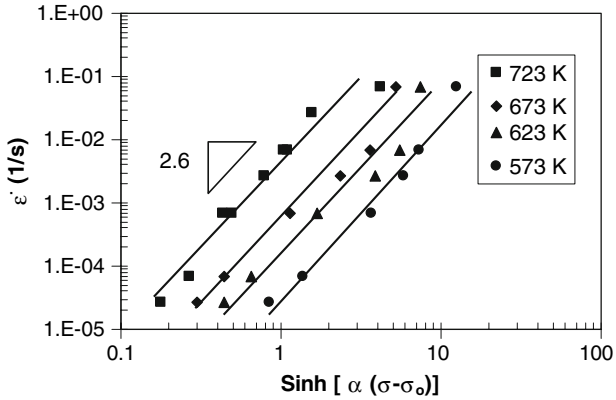

Fig. 13 Relation between $\dot{\varepsilon}$ and sinh $\alpha\sigma_e$ at various temperatures

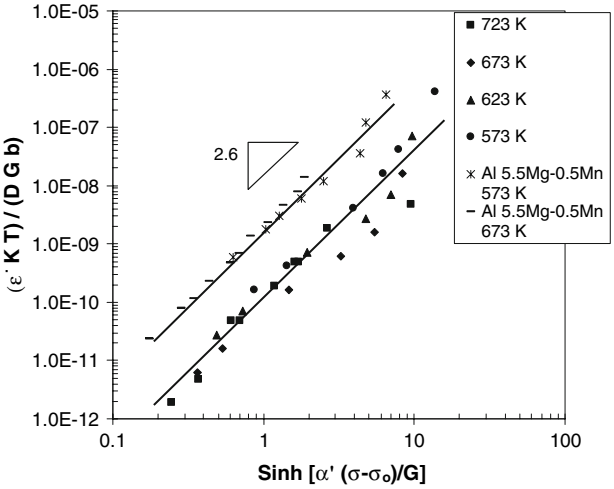

Fig. 14 Normalized strain rate vs. normalized effective stress using hyperbolic sine constitutive relation for modified 5083 alloy tested in the present study and Al-5.5 Mg-0.5Mn alloy (Ref 48)

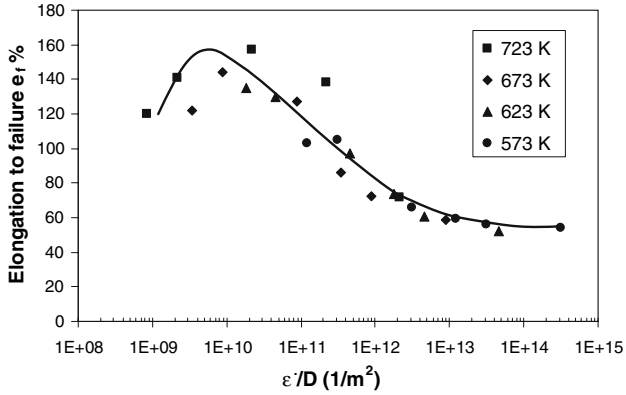

Fig. 15 Elongation to failure as a function of diffusion compensated strain rate

may also change with temperature (see the scatter of the data points for 5083 alloy at high stresses, Fig. 14). The comparison between the two alloys as presented in Fig. 14 is different from that observed before in Fig. 11. The reason for this discrepancy is due to the change in α' values. Therefore, a major disadvantage with the use of Eq 10 is that, even for alloys with similar Q values, a direct comparison between the log $(\dot{\varepsilon}kT/DGb)$ vs. log sinh $[\alpha'(\sigma-\sigma_o)/G]$ plots for different materials is misleading, since α' values may be different (Ref 36).

4.7 Ductility

The enhanced ductility in the viscous glide region is due to the high strain-rate sensitivity index m (=1/n) = 0.33. The high value of m will decrease the progression of the incipient necking. The sharp decrease in e_f% at T = 573 K is attributed to the decease in m value to ≤ 0.2 with increasing strain rate. The decrease in ductility with increasing strain rate at higher temperatures in the viscous glide region may be attributed to the intermittent breakaway of dislocation from their solute atom atmospheres as the transition strain rate to the high stress region is approached (Ref 11). It was noticed that the ductility-strain rate data in Al-3 wt% Cu (Ref 11) showed two peaks; this behavior was not observed in the present study. Figure 15 shows the relation between e_f% vs. diffusion compensated strain rate $(\dot{\varepsilon}/D)$ at various temperatures, where D is the diffusivity of Mg in Al. It can be seen in the figure that the ductility data at these temperatures are unified in a single curve that exhibits a maximum value at $(\dot{\varepsilon}/D) \sim 10^{10}$ m^{-2} (towards the lower range of strain rate in viscous glide region) and decreases to a constant plateau of 60% at $(\dot{\varepsilon}/D) \geq 10^{13}$ m^{-2}, in the region where the power law breaks down.

5. Conclusions

(1) The deformation behavior of the modified 5083 Al was examined at temperatures ranging from 573 to 723 K in the strain rate range from 10^{-5} to 10^{-1} s^{-1}. Analysis of experimental data of the alloy revealed the presence of a threshold stress that depends on temperature with an energy term, Qo, 16.5 kJ mol^{-1}.

(2) By incorporating the threshold stress into the analysis, it was shown that the deformation of the alloy can be divided into two regions. At the normalized strain rates, $\dot{\varepsilon}kT/DGb > 10^{-9}$, the stress exponent, n has a high value of $\approx$10 and the activation energy is close to that for diffusion of Mg in Al and at low normalized strain rates $\leq 10^{-9}$, the n value is 3 and the true activation energy, Q, is equal to123 kJ mol^{-1} suggesting viscous glide of dislocations as rate-controlling mechanism.

(3) Enhanced ductility was observed in the viscous glide region due to the high strain rate sensitivity in this region, with an increase in the maximum ductility with increasing temperature.

(4) The sharp drop in the ductility at high-stress region can be attributed to the decrease in strain rate sensitivity m (=0.1) at high strain rates.

Acknowledgments

This work was supported by Saudi Arabian Basic Industrial Company (SABIC) and the Research Center, College of Engineering, King Saud University under project No. 30/426. The authors gratefully acknowledged the financial support of SABIC.

References

1. O.D. Sherby and P.M. Burke, Mechanical Behavior of Crystalline Solids at Elevated Temperature, *Prog. Mater. Sci.*, 1968, **13**, p 323–390
2. A.K. Mukherjee, J.E. Bird, and J.E. Dorn, Experimental Correlation for High-Temperature Creep, *Trans. ASM*, 1969, **62**, p 155–185
3. F.A. Mohamed and T.G. Langdon, The Transition from Dislocation Climb to Viscous Glide in Creep of Solid Solution Alloys, *Acta Metall.*, 1974, **22**, p 779–788
4. M.E. Kassner and M.-T. Perez-Prado, Five-Power-Law Creep in Single Phase Metals and Alloys, *Prog. Mater. Sci.*, 2000, **45**, p 1–102
5. K.L. Murty, F.A. Mohamed, and J.E. Dorn, Viscous Glide, Dislocation Climb and Newtonian Viscous Deformation Mechanisms of High Temperature Creep in Al-3Mg, *Acta Metall.*, 1972, **20**, p 1009–1018
6. P. Yavari, F.A. Mohamed, and T.G. Langdon, Creep and Substructure Formation in an Al-5%Mg Solid Solution Alloy, *Acta Metall.*, 1981, **29**, p 1495–1507

7. M.S. Soliman and F.A. Mohamed, Correlation between Creep Behavior and Substructure in Al-3%Mg Solid-Solution Alloy, *Mater. Sci. Eng. A*, 1982, **55**, p 111–118
8. H. Oikawa, K. Honda, and S. Ito, Experimental Study on the Stress Range of Class I Behavior in the Creep of Al-Mg Alloys, *Mater. Sci. Eng. A*, 1984, **64**, p 237–245
9. H. Oikawa, H. Sato, and K. Maruyama, Influence of Temperature on the Transition of Deformation Characteristics of Al-1Mg Alloy in the Power Law Creep Regime, *Mater. Sci. Eng. A*, 1985, **75**, p 21–28
10. H. Sato and H. Oikawa, Further Experimental Study of Deformation Characteristics of Al-Mg Alloys in the Power-Law Creep Regime, *Scripta Metall.*, 1988, **22**, p 87–92
11. B. Chaudhury and F.A. Mohamed, Creep and Ductility in an Al-Cu Solid-Solution Alloy, *Metall. Trans. A*, 1987, **18**, p 2105–2114
12. B. Chaudhury and F.A. Mohamed, Creep Characteristics of an Al-2wt%Cu Alloy in the Solid Solution Range, *Mater. Sci. Eng. A*, 1988, **101**, p 13–23
13. M.S. Soliman, Effect of Cu Concentration on the Creep Behavior of Al-Cu Solid-Solution Alloys, *Mater. Sci. Eng. A*, 1995, **201**, p 111–117
14. M.S. Soliman and F.A. Mohamed, Creep Transitions in an Al-Zn Alloy, *Metall. Trans. A*, 1984, **15**, p 1893–1904
15. J. Weertman, Creep of Indium, Lead, Some of their Alloys with Various Metals, *Trans. AIME*, 1960, **218**, p 207–218
16. S. Takeuchi and A.S. Argon, Steady-State Creep of Alloys due to Viscous Motion of Dislocations, *Acta Metall.*, 1976, **24**, p 883–889
17. F.A. Mohamed, Creep Behavior of Solid Solution Alloys, *Mater. Sci. Eng. A*, 1979, **38**, p 73–80
18. F.A. Mohamed, Incorporation of the Suzuki, the Fisher Interactions in the Analysis of Creep Behavior of Solid Solution Alloys, *Mate. Sci. Eng. A*, 1983, **61**, p 149–165
19. H.J. McQueen and J.J. Jones, Recovery and Recrystallization During High Temperature Deformation, *Plastic Deformation of Materials*, R.J. Arsenault, Ed., Academic Press, New York, NY, 1975, Vol. 6, p 393-493
20. H. Nakashima, K. Iwasaki, S. Goto, and H. Yoshinaga, Combined Effect of Solution and Dispersion Hardenings at High Temperature, *Mater. Trans. JIM*, 1990, **31**(1), p 35–45
21. G. Avramovic-Cingara, D.D. Perovic, and H.J. McQueen, Hot Deformation Mechanisms of Solution-Treated Al-Li-Cu-Mg-Zr Alloy, *Metall. Mater. Trans A*, 1996, **27A**, p 3478–3490
22. E. Kovacs-Csetenyi, N.Q. Chinh, and I. Kovacs, Effect of Microstructure on Hot Deformation Characteristics of Aluminum Alloys, *Mater. Sci. Forum*, 1996, **217-222**, p 1175–1180
23. B. Ronning, K. Nord-Varhaung, T Furu, and E. Nes, The Effect of Chemical Composition and Microstructure on the Flow Stress During Hot Deformation of Aluminum Alloys, *Mater. Sci. Forum*, 2000, **331-337**, p 571–576
24. H. Zhang and H.J. McQueen, Effects Of Mn Dispersoids on Hot Working of Al-1 Mn, *Mater. Sci. Eng. A*, 2001, **319-321**, p 711–715
25. R. Kaibyshev, O. Sitdikov, I. Mazurina, and D.R. Lesuer, Deformation Behavior of a 2219 Al Alloy, *Mater. Sci. Eng. A.*, 2002, **334**, p 104–113
26. E.A. Marquis, D.N. Seidman, and D.C. Dunand, Effect of Mg Addition on the Creep, Yield Behavior of an Al-Sc Alloy, *Acta Mater.*, 2003, **51**, p 4751–4760
27. R. Kaibyshev, F. Musin, E. Avtokratova, and Y. Motohashi, Deformation Behavior of a Modified 5083 Aluminum Alloy, *Mater. Sci. Eng. A*, 2005, **392**, p 373–379
28. F.A. Mohamed, K.T. Park, and E.J. Lavernia, Creep Behavior of Discontinuous SiC-Al Composites, *Mater. Sci. Eng. A*, 1992, **150**, p 21–35
29. K.T. Park, E. Lavernia, and F.A. Mohamed., High-Temperature Deformation of 6061 Al, *Acta Metall. Mater.*, 1994, **42**, p 667–678
30. Y. Li, S.R. Nutt, and F.A. Mohamed, Investigation of Creep, Substructure Formation in 2124 Al, *Acta Mater.*, 1997, **45**, p 2607–2620
31. L. Kloc, S. Spigarelli, E. Cerri, E. Evangelista, and T.G. Langdon, Creep Behavior of an Aluminum 2024 Alloy Produced by Powder Metallurgy, *Acta Mater.*, 1997, **45**, p 529–540
32. F.A. Mohamed, Correlation Between Creep Behavior in Al-based Solid Solution Alloys, Powder Metallurgy Al Alloys, *Mater. Sci. Eng. A*, 1998, **245**, p 242–256
33. J. Čadek, S.J. Zhu, and K. Milicka, Creep Behavior of ODS Aluminum Reinforced by Silicon Carbide Particulates: ODS Al-30SiCp Composite, *Mater. Sci. Eng. A*, 1998, **248**, p 65–72
34. J. Čadek, S.J. Zhu, and K. Milicka, Threshold Creep Behavior of Aluminum Dispersion Strengthened by Fine Alumina Particle, *Mater. Sci. Eng. A*, 1998, **252**, p 1–5
35. J. Čadek, K. Kucharova, and S.J. Zhu, Disappearance of the True Threshold Creep Behavior of an ODS Al-30SiCp Composite at High Temperatures, *Mater. Sci. Eng. A*, 2000, **281**, p 162–168
36. E. Evangelista and S. Spigarelli, Constitutive Equations for Creep and Plasticity of Aluminum Alloys Produced by Powder Metallurgy and Aluminum Based Metal Matrix Composites, *Metall. Mater. Trans. A*, 2002, **33A**, p 373–381
37. Z. Lin, Y. Li, and F.A. Mohamed, Creep and Substructure in 5vol% SiC-2124 Al Composite, *Mater Sci. Eng. A*, 2002, **332**, p 330–242
38. J.S. Robinson, R.L. Cudd, and J.T. Evans, Creep Resistant Aluminum Alloys, Their Applications, *Mater. Sci. Technol.*, 2003, **19**, p 143–155
39. Y. Li and T.G. Langdon, Creep Behavior of an Al-6061 Metal Matrix Composite Reinforced with Alumina Particulates, *Acta Mater.*, 1997, **45**, p 4797–4806
40. Y. Li and T.G. Langdon, Creep Behavior of a Reinforced Al-7005 Alloy: Implication for the Creep Processes in Metal Matrix Composites, *Acta Mater.*, 1998, **46**, p 1143–1155
41. Z. Lin, S.L. Chan, and F.A. Mohamed, Effect of Nano-Scale Particles on the Creep Behavior of 2014 Al, *Mater. Sci. Eng. A*, 2005, **394**, p 103–111
42. K. Ishikawa and Y. Kobayashi, Creep and Rupture Behavior of a Commercial Aluminum-Magnesium Alloy A5083 at Constant Applied Stress, *Mater. Sci. Eng. A*, 2004, **387-389**, p 613–617
43. K. Hirano and S. Fujikawa, Diffusion of ^{28}Mg in Aluminum, *J. Nuclear Mater.*, 1978, **69-70**, p 564–570
44. S.J. Rothman, N.L. Peterson, L.J. Nowicki, and L.C. Robinson, Tracer Diffusion of Magnesium in Aluminum Single Crystals, *Phys. Status Solidi B*, 1974, **63**, p K29–K33
45. T.S. Lundy and J.F. Murdock, Diffusion of ^{26}Al and ^{54}Mn in Aluminum, *J. Appl. Phys.*, 1962, **33**, p 1671–1673
46. K. Ozturk, L-Q. Chen, and Z-K. Liu, Thermodynamic Assessment of the Al-Ca Binary System Using Random Solution and Associate Models, *J. Alloys Comp.*, 2002, **340**, p 199–206
47. H. Iwasaki, H. Hosokawa, T. Mori, and T. Tagata, Quantitative Assessment of Superplastic Deformation Behavior in a Commercial 5083 Alloy, *Mater. Sci. Eng. A*, 1998, **252**, p 199–202
48. E.M. Taleff, D.R. Lesuer, and J. Wadsworth, Enhanced Ductility in Coarse Grained Al-Mg Alloys, *Metal. Mater. Trans. A*, 1996, **27A**, p 343–352
49. K. Kucharova, L. Saxl, and J. Cadek, Effective Stress in Steady State Creep in an Al-5.5 at.% Mg Solid Solution, *Acta Metall.*, 1974, **22**, p 465–472
50. B.G. Clark, I.M. Robertson, and L.M. Dougherty, High-Temperature Dislocation-Precipitate Interactions in Al Alloys: An In situ Transmission Electron Microscopy Deformation Study, *J. Mater. Res.*, 2005, **20**(7), p 1792–1801
51. S. Spigarelli, E. Evangelista, and H.J. McQueen, Study of Hot Workability of a Heat Treated AA6082 Aluminum Alloy, *Scripta Materialia*, 2003, **49**, p 179–183